Time and layer resolved magnetic domain imagig of FeNi/Cu/Co trilayers using x-ray photoelectron emission microscopy (invited)

J. Vogel[a)]
Laboratoire Louis Néel, CNRS, 25 Avenue des Martyrs, B.P. 166, F-38042 Grenoble Cedex 9, France

W. Kuch
Max-Planck-Institut für Mikrostrukturphysik, Weinberg 2, D-06120 Halle, Germany

J. Camarero
Dpto. Física de la Materia Condensada, Universidad Autónoma de Madrid, E-28049 Madrid, Spain

K. Fukumoto
Max-Planck-Institut für Mikrostrukturphysik, Weinberg 2, D-06120 Halle, Germany

Y. Pennec[b)]
Laboratoire Louis Néel, CNRS, 25 Avenue des Martyrs, Grenoble Cedex 9, France

M. Bonfim
Departamento de Engenharia Elètrica, Universidade do Paraná, CEP 81531-990, Curitiba, Brazil

S. Pizzini
Laboratoire Louis Néel, CNRS, 25 Avenue des Martyrs, B.P. 166, F-38042, Grenoble Cedex 9, France

F. Petroff
Unité Mixte de Physique CNRS/Thales, Domaine de Corbeville, F-91404 Orsay, France

A. Fontaine
Laboratoire Louis Néel, CNRS, 25 Avenue des Martyrs, B.P. 166, F-38042, Grenoble Cedex 9, France

J. Kirschner
Max-Planck-Institut für Mikrostrukturphysik, Weinberg 2, D-06120 Halle, Germany

(Presented on 6 January 2004)

We have performed magnetic domain imaging with spatial, temporal, and layer resolution using x-ray photoelectron emission microscopy. The element selectivity of x-ray magnetic circular dichroism allows the magnetization dynamics of the different magnetic layers in spin-valve-like FeNi/Cu/Co trilayers to be studied separately, using the time structure of synchrotron radiation. The unique possibilities of this technique have been used to study the influence of the intrinsic magnetic properties of the different layers on the magnetization dynamics and the interlayer magnetic coupling. © *2004 American Institute of Physics.* [DOI: 10.1063/1.1676027]

The dynamics of magnetization reversal in thin magnetic films is an important issue in physics today, since it determines the speed with which information can be read and written in magnetic storage devices. Examples of devices for which this speed is important are spin-valves, which are commonly used in magnetic read heads, and magnetic tunnel junctions, which are very promising as memory cells in magnetic random access memories.[1] These devices consist of several thin magnetic layers coupled through nonmagnetic spacers, and the behavior of the magnetization as a function of time and field is often not the same for the different layers.

Very few experimental techniques can address the magnetic behavior of the different layers separately. One of the most powerful is x-ray magnetic circular dichroism (XMCD), which uses the element selectivity of x-ray absorption edges combined with the magnetic sensitivity of circularly polarized x-rays. This technique can be used to gain information about the average size and direction of spin and orbital magnetic moments in each of the atomic species constituting a magnetic heterostructure. We have recently used time-resolved XMCD to probe the layer resolved magnetization dynamics of FeNi/Cu/Co spin-valves deposited on step-bunched Si(111) substrates, using nano-second long magnetic field pulses.[2] These measurements showed that the magnetic coupling between the FeNi and Co layers through the Cu spacer was strongly reduced in dynamic conditions with respect to the quasistatic regime. In order to get a complete understanding of the magnetization reversal dynamics in this kind of trilayers, it is necessary to add spatial resolution to the layer selectivity. This can be done using x-ray microscopy techniques, like x-ray photoelectron emission microscopy (X-PEEM).[3] X-ray imaging techniques have already been used to study magnetization dynamics,[4–6] but until now the layer selectivity had not been explored. In this article, we present layer resolved microscopy measurement of magnetization dynamics in spin-valve-like trilayer structures.

At the atomic scale, magnetization dynamics is governed by the Landau–Lifshitz–Gilbert equation of precession and damping. This equation can still be applied for small mag-

[a)]Electronic mail: vogel@grenoble.cnrs.fr
[b)]Present address: Department of Physics, University of Alberta, Edmonton, Alberta, Canada T6G 2J1.

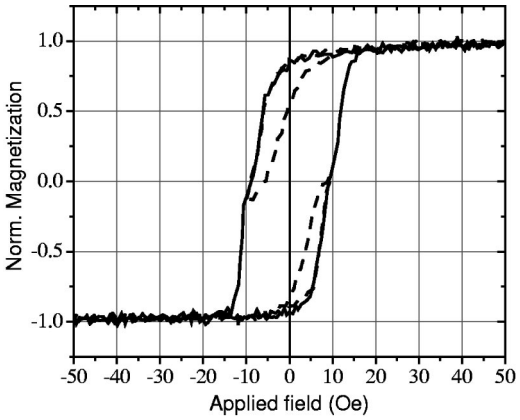

FIG. 1. Major and minor hysteresis curves obtained by longitudinal Kerr effect for the $Fe_{20}Ni_{80}$(5 nm)/Cu(4 nm)/Co(5 nm) spin-valve-like trilayer deposited on $Si(100)/SiO_2$. No magnetic anisotropy in the plane of the sample was observed. Minor curves of the FeNi layer are indicated with a dashed line: they show the coupling between the permalloy layer (lower coercivity) and the Co layer (higher coercivity).

netic structures, where the spins reverse more or less coherently, and the precession and an adequate tailoring of the magnetic pulse can be used to have extremely short reversal times of some hundreds of picoseconds.[7] Above lateral sizes of some micrometers, the reversal becomes thermally activated and it proceeds through nucleation of reversed domains and/or propagation of domain walls. The reversal mode can strongly depend on the speed at which the applied field is changed and, in return, the magnetic coupling can be different for the different reversal modes.

The sample investigated in this article is a $Fe_{20}Ni_{80}$(5 nm)/Cu(4 nm)/Co(5 nm) trilayer deposited at normal incidence on a $Si(100)/SiO_2$ substrate by rf sputtering. A capping layer of 3 nm of Al was deposited for protection against oxidation. The magnetization of the sample lies in the plane of the layers and no preferential magnetization axis exists within this plane. The magnetization curve for the sample is shown in Fig. 1. Two transitions are visible, indicating a separate reversal for the two magnetic layers, the permalloy layer having the lower coercivity. Due to the coupling with the Co layer, the minor curve of the permalloy layer is shifted with respect to zero field. This coupling is mainly due to correlated roughness at the two F/NM interfaces, which gives rise to the so-called Néel orange peel coupling.[8] The magnetic transitions are not square but tilted, due to the absence of anisotropy but also due to the presence of many pinning centers, as will be shown later. In the following, we will show how these intrinsic magnetic properties affect the coupling and the magnetization reversal in the two layers.

The time- and layer-resolved magnetic images of our sample were obtained combining XMCD and x-ray photoemission electron microscopy (X-PEEM). XMCD is the dependence of x-ray absorption on the relative orientation of the local magnetization direction and the polarization vector of the circularly polarized x-rays. In X-PEEM, the secondary electrons emitted by the sample surface after x-ray absorption are used to create a magnified image of the sample. The number of emitted secondary electrons is proportional to the local absorption. In a trilayer system in which two ferromagnetic (FM) layers are separated by a nonmagnetic or an antiferromagnetic spacer layer, the domain patterns in the two FM layers, as well as their correlation and interaction, can be observed separately.[9–11]

Our time-resolved X-PEEM measurements were performed at the UE52 helical undulator beamline of BESSY II in Berlin. The setup of the electrostatic photoelectron emission microscope (Focus IS-PEEM) is identical to that described in previous publications.[9] The angle of incidence of x-rays on the sample was 60° from the surface normal. The spatial resolution was set to 300 nm, and the field of view to 25 μm.

Temporal resolution can be obtained exploiting the pulsed nature of the x-ray photons, resulting from the bunches of electrons circulating in the storage ring. In single bunch mode operation of BESSY, photon bunches are emitted with a repetition rate of 1.25 MHz (800 ns separation between bunches). Our measurements were performed in a stroboscopic pump-probe mode, synchronizing magnetic field pulses with the x-ray photon bunches. To reduce the power supplied by our pulsed current source, a magnetic pulse was provided only every second photon pulse (1.6 μs between pulses), using the technique described in our previous article.[6] Magnetization reversal dynamics was then studied as a function of time, during and after the magnetic pulse, by changing the delay between magnetic and photon pulses. A complete description of the experimental setup can be found in Ref. 6.

The technical challenges of time-resolved X-PEEM are considerable. A major difficulty for measurements of magnetization dynamics using this technique is the sensitivity of secondary electron trajectories to the applied magnetic field. In order to avoid important displacements of the magnetic image in the microscope, the magnetic stray field outside the sample has to be minimized. The sample was therefore set at the inner surface of a double stripline copper coil, made of 12.5 μm thick Cu foil. A hole of 1×3 mm^2 was made in the top line, exposing the imaged sample surface. The sample was in electrical contact with the Cu sample holder using two molybdenum clamps. A schematic drawing of the experimental geometry is given in the inset of Fig. 2.

The current pulses used to create the magnetic field were provided by a water-cooled homemade current driver[12] based on fast power metal-oxide-semiconductor field effect transistors, located outside the vacuum chamber. A low impedance coaxial cable made of two 12.5-μm-thick and 15-mm-wide copper strips was used to transmit the current pulse from the current driver to the coil. The current driver was able to supply pulses with a current up to 90 A and a length up to several hundreds of nanoseconds. The strength of the magnetic field, calculated from the geometry and the current in the coil, was 7 Oe per ampere of current. The field strength was also calibrated using the Faraday rotation of a paramagnetic sample with known Verdet constants, agreeing with the calculated values within 10%. Due to the deviation of the secondary electrons by the applied magnetic field, PEEM images taken during the field pulse are shifted with respect to images taken without field. This shift can be used as a direct measure of the field strength on the sample, and corresponds

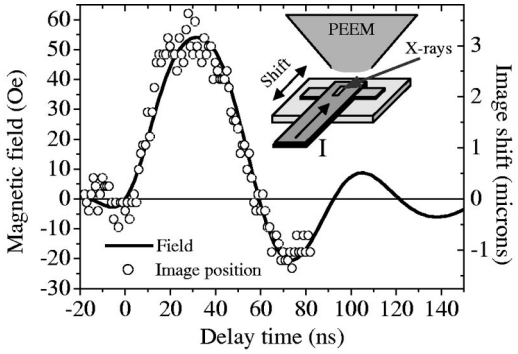

FIG. 2. Current in the microcoil (line) and equivalent magnetic field (left axis) using a conversion of 7 Oe/A, and relative shift of the image position in microns (symbols, right axis), for a pulse with a length of 60 ns and a maximum current of 7.8 A. A schematic drawing of the measuring geometry, indicating the incident light direction and the direction of the image shift, is given in the inset. The image shift is proportional to the local field at the sample position and is in good agreement with the measured current.

well with the shape of the current pulse. An example is shown in Fig. 2. The continuous line is a measure of the current in the coil for a bipolar pulse with a length of 60 ns and a current of 7.8 A in the maximum. On the left axis, the equivalent field value is given, using the conversion of 7 Oe/A. The white symbols give the shift of the image in micrometers (right axis) with respect to the position at zero field. This shift was measured using the position of a topological defect on the surface of the sample. As the field is localized close to the sample, the shift is relatively small compared with the field of view (about 4 μm maximum for a field of view of 25 μm). Correcting this shift might become a serious challenge if a better resolution, and therefore a smaller field of view, needed to be used.

Layer-resolved PEEM images of the permalloy and Co layers of the spin-valve are shown in Figs. 3 and 4. The x-ray energy was tuned to the Fe L_3 absorption maximum to image the permalloy layer, while for the Co layer the maximum of the Co L_3 absorption was used. The permalloy layer contains

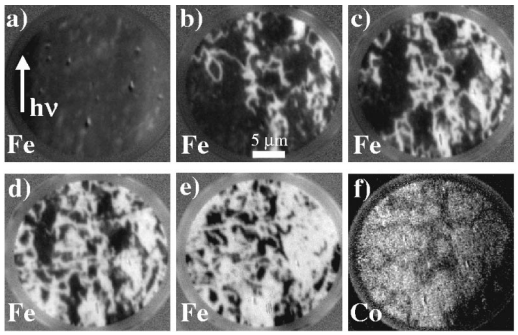

FIG. 3. Static layer resolved X-PEEM images (diameter 25 μm) of the magnetization state of the permalloy [(a) to (e)] and Co (f) layers. The projection of the x-ray incidence direction on the sample surface is pointing up in the images (parallel to the arrow) and is parallel/antiparallel to the direction of the field for positive/negative pulses. The magnetization direction points up (parallel to the arrow) for black domains, while it points down for white domains. The images were taken after applying different numbers of 18 ns long and 100 Oe strong negative pulses to the sample. The total number of pulses is 0 (a), 1 (b), 2 (c), 4 (d), and 10 (e and f). The domains are small and irregular, due to the absence of magnetic anisotropy and a high density of pinning centers.

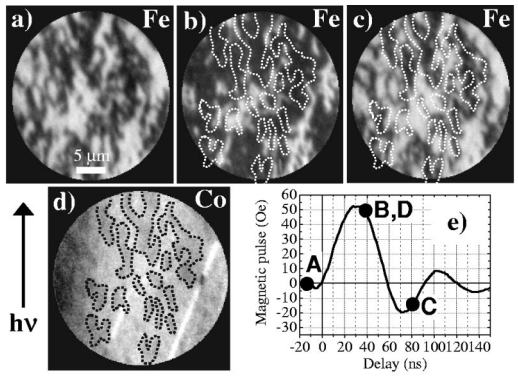

FIG. 4. Time and layer-resolved X-PEEM images (diameter 25 μm) for the magnetization state of the permalloy [(a) to (c)] and Co (d) layer. The projection of the x-ray incidence direction on the sample surface is pointing up in the images (parallel to the arrow) and is parallel/antiparallel to the direction of the field for positive/negative fields. The magnetization direction points up (parallel to the arrow) for black domains, while it points down for white domains. The permalloy images were taken at different time delays with respect to the magnetic pulse, indicated in (e). The most clearly visible black domains in the Co layer are denoted with dotted white lines on the permalloy images in (b) and (c). The correlation between the permalloy and Co domain structures is most clearly seen comparing (c) and (d): the permalloy is mainly black where the Co is black and mainly white where the Co is white.

four times more Ni than Fe, leading one to expect that a better image intensity could be obtained using the Ni L_3 absorption maximum. We found, however, that the Fe L_3-edge energy gave a better signal to noise ratio. The absorption cross section at the Fe L_3 absorption maximum is about two times higher than at the Ni L_3 maximum. In addition, the dichroic asymmetry (difference normalized by peak height) of Fe is at least 50% higher than that of Ni.[13] Moreover, the flux at the UE52 beamline is about 50% higher at the Fe L_3 energy than at the Ni L_3 energy. The images, obtained at room temperature, represent the asymmetry (difference divided by sum) of two measurements taken with left and right photon helicities. The contrast is due to the different absorption of regions of the sample having their magnetization parallel and antiparallel to the incoming x-ray's direction. The projection of the x-ray incidence direction on the sample surface is pointing up in the images and is parallel/antiparallel to the direction of the field for positive/negative pulses: The magnetization direction points up for black domains, while it points down for white domains.

In Fig. 3, we first present some static layer-resolved PEEM images of the permalloy and Co layers. These static images were taken to study the evolution of the domain structure in the sample during the first few pulses. The first image, Fig. 3(a), shows the permalloy layer that is almost saturated in the up direction. Starting from this almost saturated state, we applied several subsequent, short magnetic pulses to the sample in the down direction, with a length of 18 ns and an amplitude of 100 Oe. After every magnetic pulse, the current source was switched off and images were taken of the permalloy as well as the Co layer. In Figs. 3(b)–3(e), images of the permalloy layer taken after a total of one, two, four, and ten single magnetic pulses are shown. Figure 3(f) gives an image of the Co layer after ten pulses, corresponding to the permalloy image in Fig. 3(e). The contrast is

weaker in the Co images, since the electrons emitted by the Co layer have to travel through a total thickness of 12 nm of Cu, FeNi, and Al before reaching the surface. The number of electrons coming from the Co layer is therefore much smaller than for the permalloy, leading to a smaller signal to noise ratio.

During the first pulse, many small white domains have appeared in the permalloy layer, as seen in Fig. 3(b). The domains are very irregular, due to the absence of anisotropy in the plane. After the second pulse [Fig. 3(c)], some more domains have appeared, but the lateral size of the existing domains hardly increases. A clear increase of the total reversed area is visible after a total of four pulses, Fig. 3(d), and ten pulses, Fig. 3(e), but the general morphology of the domains does not change. Applying more pulses did not significantly change the domain structure. The domain structure is labyrinth-like, with a maximum domain width of some microns and many persisting unreversed black domains. The domain wall movement is strongly blocked, indicating a large density of pinning centers. In Fig. 3(f) a similar labyrinth-like structure is visible in the Co layer, but with larger domain sizes. Some correlation between the domain structures in the two layers seems to be present [Figs. 3(e) and 3(f)], most clearly in the zone in the top center of the image that is mainly black in both layers. In summary, these images indicate that the application of short magnetic pulses to this sample induces a strongly pinned labyrinth-like domain structure that becomes stable after several pulses.

Time- and layer-resolved images are presented in Fig. 4. The applied bipolar pulses had a maximum field strength of 55 Oe, a length of 60 and 30 ns for the positive and negative field pulses, respectively, and a risetime of about 20 ns. The field as a function of time is shown in Fig. 4(e). Before starting to apply the pulses, the sample was saturated in the down (white) direction. The images of the permalloy layer domain structure obtained before the field pulse and at the maximum of the positive and the negative pulses are reported in Figs. 4(a) to 4(c). The contrast in the images is as good as in the static images of Fig. 3, indicating that the magnetization reversal is reproducible. At the maximum of the field, some white domains in the permalloy layer are blocked on defects. These defects are clearly visible in Fig. 4(d), which shows the Co domain structure at 40 ns after the beginning of the pulses. We observed no difference between Co images taken in the maximum and minimum of the field. The reversal of the permalloy layer takes place mainly through propagation of existing domain walls. Some domains seem to appear going from B to C, but we cannot exclude that these domains are still present in Fig. 4(b) but are too small to be seen on this scale. Our images indicate that it is very hard to saturate the magnetization of this sample with short pulses, due to a great number of 360° domain walls.

The strong pinning of the domain walls also has an influence on the effective coupling between the permalloy and Co layers. The contour of the most clearly visible black domains in the Co layer [Fig. 4(d)] has been transposed to the permalloy images in Figs. 4(b) and 4(c), showing that the permalloy shows mainly black domains in this region as well, independently of the external field strength. In Fig. 4(b), the external field is pointing in the up (black) direction. In the regions where the external field and the local coupling are parallel (black domains in the Co layer), the permalloy is almost completely black. In the regions where they are opposite (white domains in the Co layer), many white domains persist in the permalloy layer. Part of the white domains seems to be blocked on some scratches on the sample, clearly visible in the Co image. In Fig. 4(c), the external field is pointing down. In this case, the external field and the local field induced by the coupling with the Co layer are parallel in the white regions of the Co. However, many black domains seem to persist above the white domains in the Co. This shows that the local coupling with the Co has an important influence on the reversal of the permalloy layer, but that local pinning fields in the permalloy layer determine the exact domain pattern.

These results show that the local coupling as well as the intrinsic properties have to be taken into account to explain the details of magnetization reversal in these thin films. Note that the coercivity of the permalloy layer in dynamic conditions increases almost an order of magnitude with respect to the quasistatic measurements. This fast increase of the coercivity is typical of thermally activated reversal and depends on the activation volume for domain wall motion, which is strongly related to the density and strength of pinning centers. In our future measurements, we will investigate the influence of intrinsic properties like interface roughness and magnetic anisotropy on the fast reversal and dynamic coupling in this kind of trilayer systems.

We thank A. Vaurès for sample preparation. Financial support by BMBF (No. 05KS1EFA6), EU (BESSY-EC-HPRI Contract No. HPRI-1999-CT-00028) and the Laboratoire Européen Associé ''Mesomag'' is gratefully acknowledged.

[1] G. A. Prinz, Science **282**, 1660 (1998).
[2] M. Bonfim, G. Ghiringhelli, F. Montaigne, S. Pizzini, N. B. Brookes, F. Petroff, J. Vogel, J. Camarero, and A. Fontaine, Phys. Rev. Lett. **86**, 3646 (2001).
[3] C. M. Schneider and G. Schönhense, Rep. Prog. Phys. **65**, R1785 (2002).
[4] P. Fischer, G. Denbeaux, H. Stoll, A. Puzic, J. Raabe, F. Nolting, T. Eimuller, and G. Schütz, J. Phys. IV **104**, 471 (2003).
[5] A. Krasyuk, A. Oelsner, S. A. Nepijko, C. M. Schneider, and G. Schönhense, Appl. Phys. A: Mater. Sci. Process. **76**, 863 (2003).
[6] J. Vogel, W. Kuch, M. Bonfim, J. Camarero, Y. Pennec, F. Offi, K. Fukumoto, J. Kirschner, A. Fontaine, and S. Pizzini, Appl. Phys. Lett. **82**, 2299 (2003).
[7] H. W. Schumacher, C. Chappert, P. Crozat, R. C. Sousa, P. P. Freitas, J. Miltat, J. Fassbender, and B. Hillebrands, Phys. Rev. Lett. **90**, 017 201 (2003); H. W. Schumacher, C. Chappert, R. C. Sousa, P. P. Freitas, and J. Miltat, *ibid.* **90**, 017 204 (2003).
[8] L. Néel, C.R. Acad. Sci. Paris **255**, 1676 (1962).
[9] W. Kuch, R. Frömter, J. Gilles, D. Hartmann, Ch. Ziethen, C. M. Schneider, G. Schönhense, W. Swiech, and J. Kirschner, Surf. Rev. Lett. **5**, 1241 (1998).
[10] W. Kuch, Appl. Phys. A: Mater. Sci. Process. **76**, 665 (2003).
[11] W. Kuch, X. Gao, and J. Kirschner, Phys. Rev. B **65**, 064 406 (2002).
[12] K. Mackay, M. Bonfim, D. Givord, and A. Fontaine, J. Appl. Phys. **87**, 1996 (2000).
[13] J. Stöhr, J. Electron Spectrosc. Relat. Phenom. **75**, 253 (1995).